Journal of Peptide Science
*J. Peptide Sci.* **9**: 177–186 (2003)
Published online in Wiley InterScience (www.interscience.wiley.com). DOI: 10.1002/psc.444

JOURNAL OF PEPTIDE SCIENCE

# Effect of pH on the Aggregate Formation of a Non-Amyloid Component (1–13)

**HIROSHI ABE[a,b] and HIROSHI NAKANISHI[a,b]***

[a] Biological Information Research Center, National Institute of Advanced Industrial Science and Technology, 1-1 Higashi, Tsukuba, Ibaraki 305-8566, Japan
[b] Department of Biological Science and Technology, Tokyo University of Science, 2641 Yamazaki, Noda, Chiba 278-0022, Japan

*Received 7 August 2002*
*Accepted 17 September 2002*

Abstract: The formation of aggregates including amyloid fibrils in the peptide fragment of non-amyloid-$\beta$ component (NAC(1–13)) was investigated under a variety of solution conditions. Two types of sample preparation method from neutral and acidic conditions were examined. Electron microscopy observation showed amorphous aggregates in the sample at pH 4.5 adjusted from the neutral condition. The CD and HPLC quantitative analyses indicated that the formation of the amorphous aggregate did not accompany a conformational conversion from a random coil in the sample solution. The analyses of p$K_a$ values determined by pH titration experiments in NMR spectroscopy indicated that the protonation of the carboxyl group of the *N*-terminal glutamic acid triggers the aggregation of NAC(1–13). On the other hand, electron microscopy observation showed that the samples at pH 2.2 and 4.5 adjusted from an initial pH of 2.2 form fibrils. A $\beta$-structure was detected by CD spectroscopy in the 1 mM NAC(1–13) at pH 2.2 immediately after preparation. The CD analyses of samples at different concentrations and temperatures indicated that 1 mM NAC(1–13) immediately after preparation at pH 2.2 was oligomerized. The quantity of the $\beta$-structure was increased depending on the incubation time. The results strongly suggested that the $\beta$-conformational oligomers play a critical role for the fibril nucleus. 

Keywords: amyloid fibril; $\alpha$-synuclein; electron microscopy; circular dichroism; NMR; aggregation; conformational conversion; non-amyloid $\beta$ component

## INTRODUCTION

A number of diseases are known as conformational diseases and seem to be characterized by the slow conformational conversion of peptides and proteins into an insoluble $\beta$-sheet form [1,2].

A non-amyloid component (NAC) is one of the fibrous peptides [3–6] that was identified as the second major component in the amyloid purified from the brain tissue of Alzheimer's disease patients [7]. NAC is also known as a peptide fragment of $\alpha$-synuclein (residues 61–95) [7]. In addition to its role as a seed for amyloid formation of amyloid $\beta$-peptide (A$\beta$) [8], NAC is supposed to be a region responsible for the aggregation and neurotoxicity of $\alpha$-synuclein as the major constituent of the Lewy body in patients with Parkinson's disease [9–12].

NAC has a hydrophobic amino acid sequence of the GAVV motif within NAC(8–11). The GAXX motif, in which X is an amino acid residue with an aliphatic side chain, has been identified not only in NAC but also in several amyloidogenic proteins [5,8] that is, GAVV in prion protein (119–122), GAII in A$\beta$(29–32) and GAIL in islet amyloid polypeptide (24–27). These analogies in the peptide sequences suggest the ability to form fibril by the fragment

*Correspondence to: Dr Hiroshi Nakanishi, Tsukuba Central 6, 1-1, Higashi, Tsukuba, Ibaraki 305-8566, Japan;
e-mail: hiroshi-nakanishi@aist.go.jp

peptide of NAC with a GAVV sequence. But an earlier study by Bodles *et al.* [6] reported that the CD spectra of trideca-peptide NAC(1–13) and nona-peptide NAC(6–14) with a GAVV motif did not indicate a $\beta$-sheet secondary structure, and electron microscopy (EM) observation showed few fibrils. In their study, however, the pH condition was not changed. For the study of peptide and protein aggregation, extremely low pH conditions have often been used [13–15], and it is also well known that the pH of the solution plays a critical role in the construction of the higher-order structure of fibrous proteins [16–18].

In this study, our attention was focused on the relationship between the pH of the solution and the higher-order structure of NAC(1–13) (EQVT-NVGGAVVTG) as a model peptide of aggregation and fibril formation. The aggregation mechanism of NAC(1–13) was discussed based on two sample conditions adjusted from acidic or neutral solutions.

## METHODS

### Peptide Synthesis

NAC(1–13) was synthesized by Fmoc strategy using a simultaneous multiple peptide synthesizer, Model PSSM-8 (Shimadzu Corp, Kyoto Japan). Each residue was coupled for 30 min with PyBOP/HOBt (Watanabe Chemical Industries, Hiroshima, Japan). The peptide was cleaved from an Alko-resin (Watanabe Chemical Industries, Hiroshima Japan) using 5% anisole and 1% 1,2-ethanedithiol in trifluoroacetic acid for 1.5 h at room temperature. The cleaved peptide was washed with diethyl ether and solubilized with 25% acetonitrile in 0.01 N HCl.

Crude NAC(1–13) was purified by reverse-phase HPLC using an ODS column (20 mm × 150 mm) heated at 40 °C with a linear gradient of 20% to 25% acetonitrile in an aqueous solution of 0.01N HCl for 10 min at a flow rate of 9.9 ml/min. The molecular weight of the peptide was determined by a matrix-assisted laser desorption/ionization time-of-flight mass spectrometry (MALDI-TOF MS). The $(M + H)^+$ value of NAC(1–13) was calculated to be 1231.4, and found to be 1231.7. The peptide purity was greater than 95% by analytical HPLC. Purified peptides were lyophilized and stored at −20 °C until used.

### Preparation of Peptide Samples

The sample of the synthetic fragment peptide NAC(1–13) in this study was dissolved in 10 mM phosphate-buffered solution, because the p$K_{a1}$ (2.1) and p$K_{a2}$ (7.2) of phosphoric acid are convenient for setting the initial pH of the solution at acidic and neutral conditions. Moreover, there is an advantage for NMR measurement in using the phosphate solution because the proton signals of phosphoric acid are not observed in the spectra. Although pH 4.5 is out of the buffer range of phosphoric acid, 10 mM phosphate solution was used for all examinations to avoid any effect on peptide conformational change resulting from using different buffers [18]. After incubation for 1 week at 37 °C, the pH of the sample at 4.5 was shifted +0.02 for the sample with the pH adjusted from acidic pH, and +0.16 from neutral pH. The pH values immediately after sample preparation are described in the electron microscopy (EM), CD and HPLC measurements.

Concentrated phosphate solutions (100 mM) at pH 1.6 and 9.2 were used as the buffer for the sample preparations. For the acidic sample, 100 mM phosphate buffer of pH 1.6 was used, and the solution was centrifuged at 2300 × **g** for 10 min to remove debris. For the neutral sample, 100 mM sodium phosphate buffer of pH 9.2 was used because the synthesized peptide is acidic due to the hydrochloride salt form. The sample solution was filtered with a 450 nm membrane filter (Millex-HV, Millipore).

All pH measurements were performed with a HM-30V pH meter (TOA, Japan) with an electrode for 5 mm NMR tubes (GST-5428S, TOA, Japan). Standard aqueous buffers were used for electrode calibration at pH 4 and 7.

### Electron Microscopy

To observe the aggregate of NAC(1–13) by EM, peptide samples (1 mM) in 10 mM sodium phosphate buffer were incubated for 1 week at 37 °C.

A droplet of each sample was put on a 400 mesh copper grid (Veco, The Netherlands) coated with collodion, negatively stained with 1% uranylacetate for about 1 min, and excess staining solution was removed with filter paper. The specimens were allowed to dry, then coated with carbon in a vacuum evaporator (JEE-400, Jeol, Japan) and observed by transmission EM (JEM-1230, Jeol, Japan) operated at 75 kV.

### Congo Red Staining and Birefringence

A sample of 1 mM NAC(1–13) dissolved immediately at pH 2.2 was incubated for 1 week at 37 °C. The

 

aggregated peptide was washed three times by pure water with a centrifugal filter with a cut-off at 100 kDa (Ultrafree-MC, Millipore), and then freeze-dried. Staining was performed by the addition of a solution of 500 μM Congo red in 100 mM NaCl and 10 mM sodium phosphate buffer (pH 7.4). The mixture was incubated for 30 min at 37 °C and then centrifuged. The resultant pellet was placed on a slide and examined under polarizing light using a Nikon Optiphot-pol microscope under a 10× lens.

### Circular Dichroism Spectra

The CD spectra were recorded on a Jasco J720 spectropolarimeter from 250 to 180 nm, taking points every 0.2 nm with a 2 s integration-time and a 1 nm bandwidth. Four scans were averaged. All spectra were corrected by subtracting the baseline of the buffer solution recorded under the same condition. Quartz cells with 0.1–1 mm pathlengths were used. The CD absorbances were expressed as the mean residue ellipticity [$\theta$] in units of degrees $cm^2$ $dmol^{-1}$.

Temperatures were controlled with a refrigerated bath and circulator (Haake, DG-8), and read by a resistance thermometer sensor (Chino DB1000). Temperatures were changed within 25°–90 °C at 5 °C intervals every 15 min.

### Quantification of Solute in Sample Solution

To quantify the solute in the sample solution, samples were filtered with a 220 nm centrifugal filter (Ultrafree-MC, Millipore) at 4500 × **g** for 20 min. The $\theta_{198}$ intensities in CD spectra were obtained by averaged $\theta$ values over the wavelength range of 199 to 197 nm to reduce the experimental errors. Filtrates were applied to HPLC under the same condition as peptide purification. Peak areas were calculated by an adjunctive computer unit of C-R7A plus (Shimadzu, Japan).

### Dynamic Light Scattering Experiments

Measurements of dynamic light scattering were performed at 25 °C with a submicron particle sizer Nicomp model 370 (Nicomp, CA, USA) and a helium-neon laser (632.8 nm). The scattering angle was 90°. Measurements were performed within 2–5 min.

### NMR Experiments

Peptide samples for NMR measurements were dissolved in $H_2O/D_2O$ 9 : 1 (v/v) with 10 mM sodium phosphate and a minute amount of phosphoric acid was added to adjust the samples for acidic pH. Sodium 3-(trimethylsilyl)-propane sulfonate in a capillary tube was used as the standard for NMR chemical shifts.

The NMR spectra were acquired using a Bruker DMX750 spectrometer. The resonance peaks of the peptide were assigned using the usual 2D-NMR techniques [19].

### pH Titration of $^1$H NMR Chemical Shifts of NAC(1–13)

Chemical shifts of E1 H$\alpha$, E1 H$\gamma$ and G13 H$\alpha$ in NAC(1–13) were analysed to determine p$K_a$ values for the *N*-terminal amide group of E1, the carboxyl group of E1 and the *C*-terminal carboxyl group, respectively.

2D TOCSY experiments were performed at twelve different pH values between 2.1 and 10.0. Twelve E1H$\alpha$ resonances between pH 2.1 and 10.0, nine E1H$\gamma$ resonances between pH 2.1–6.7 and eleven G13H$\alpha$ resonances between pH 2.1–9.4 were used for nonlinear least-squares analysis. The NMR spectra were recorded at 25 °C. The pH of the sample was read before and immediately after the NMR experiments, and the latter measurement was applied to pH titration calculations.

p$K_a$ values were calculated by nonlinear least-squares fitting using the data analysis program Origin (Microcal Software, Inc.) of experimental pH titration curves to the following equation:

$$\delta = [\delta_{acid} + \delta_{base} 10^{(pH-pK_a)}]/[1 + 10^{(pH-pKa)}] \quad (1)$$

where $\delta_{acid}$ and $\delta_{base}$ represent chemical shifts at low and high extremes of pH, respectively. The equation was derived from the Henderson–Hasselbach equation assuming a rapid equilibrium between protonated and unprotonated forms [20].

## RESULTS AND DISCUSSION

### The Morphology of the NAC(1–13) Aggregate Depending on the pH of the Sample Immediately after Dissolution and Incubation

Two different pH solutions were used for the sample in the experiments. One solution, the pH immediately after the sample dissolution was ca. 2.2 and another solution, the pH immediately after the sample dissolution was ca. 7.5.

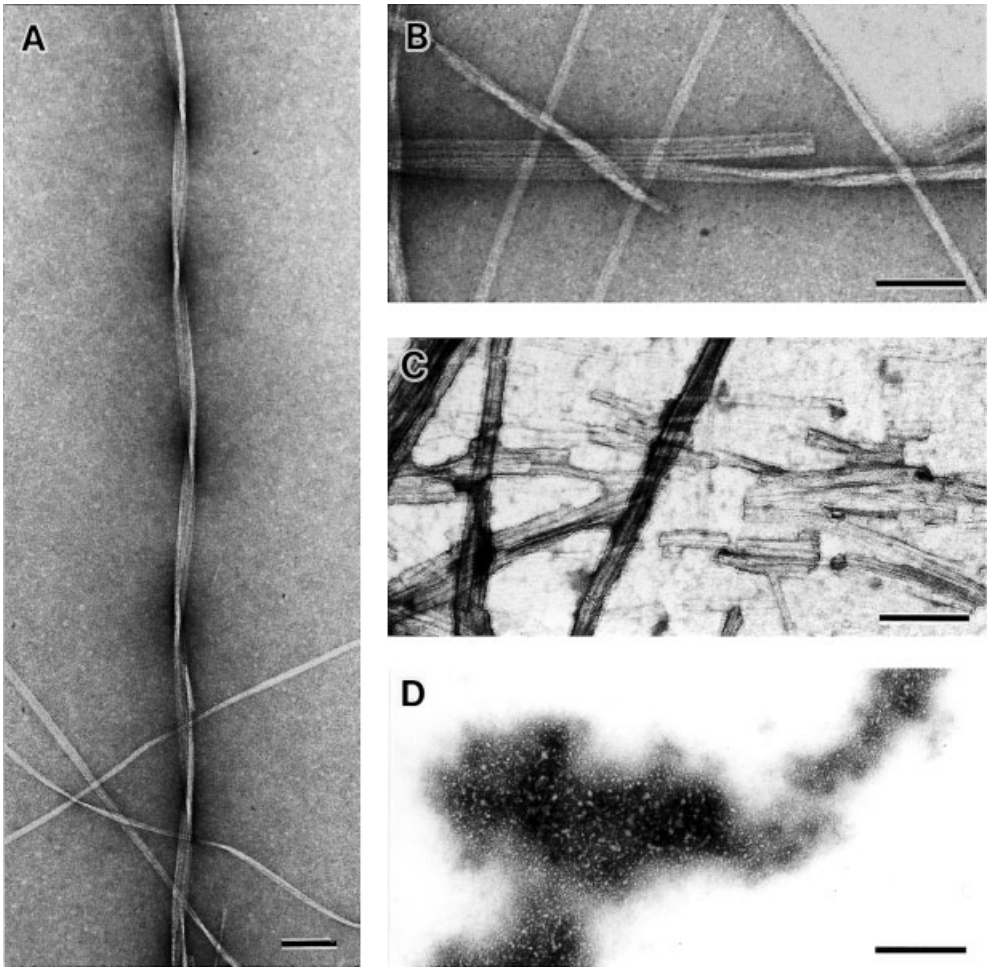


Figure 1 Electron micrographs of NAC(1–13). 1 mM sample solutions were incubated for 1 week at 37 °C. (A, B) Solution pH immediately after sample dissolution is pH 2.2. Figure (A) contains twisted fibril and (B) flat ribbons. (C) Solution pH was adjusted to pH 4.5 with small aliquots of NaOH solution from pH 2.2. (D) Solution pH was adjusted to pH 4.5 using small aliquots of phosphate from pH 7.5. Scale bars represent 100 nm.

Figure 1 shows the electron micrographs of 1 mM NAC(1–13) after incubation at 37 °C for 1 week. The acidic samples dissolved immediately at pH 2.2 showed twisted and untwisted fibrils (Figure 1A), and a flat ribbon structure with a variety of widths (5–60 nm, Figure 1B). These fibrils and ribbons seem to be composed of narrower protofilament (ca 5 nm). The result showed that the NAC(1–13) is the shortest fibril-forming peptide among the previously reported NAC fragments [5,6]. Some fibrils and ribbons were twisted. Although no constant axial periodicity was found in the twisted fibrils, a positive correlation was displayed between a helical pitch (including two twists) of fibrils and the average width of the fibrils as shown in Figure 2. The widths of fibrils were measured in the middle of twist, and the width values in a helical pitch were averaged.

The Congo red stained sample exhibited yellow–green birefringence under polarized light, indicating that the aggregate of 1 mM NAC(1–13) immediately dissolved at pH 2.2 is amyloid fibril (data not shown).

The sample at pH 4.5, adjusted from the acidic condition at pH 2.2, showed untwisted and typically shorter fibrils (Figure 1C) than those which were observed at pH 2.2 (Figure 1A,B). In spite of the same pH condition at 4.5, the samples whose pHs were adjusted from the neutral condition showed amorphous precipitates in EM (Figure 1D) and visible aggregates in the solution were seen by the naked eye. Almost no fibrils were observed. The result of EM observation of the sample prepared from the neutral condition probably corresponds to the previous report of Bodles *et al.* [6]. These results

 

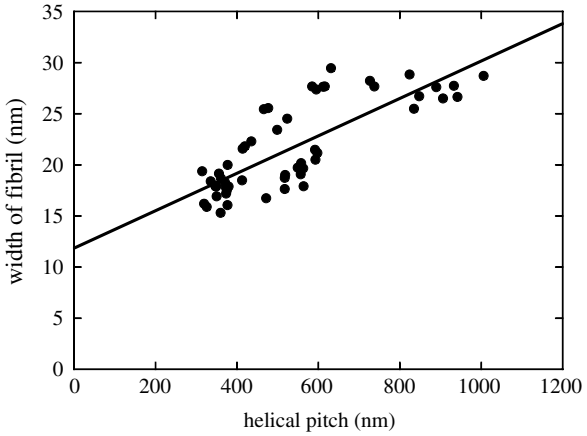


Figure 2 A total of 52 average widths of fibril were plotted as a function of helical pitch (including two twists). The line corresponds to the average width of fibril = (0.0183 × helical pitch of fibril) + 11.9 ($\chi^2 = 0.63$).

described above indicate that the aggregate forms of NAC(1–13) strongly depend on the pH conditions immediately after the sample dissolution.

## Aggregation Process of NAC(1–13) with the pH Adjusted from Neutral Condition

In order to elucidate the difference in aggregation mechanisms between the samples with the pHs adjusted from neutral and more acidic pH, detailed CD analyses of NAC(1–13) were performed using two different sample conditions.

The neutral sample solution of NAC(1–13) (pH 7.5) was prepared using 10 mM sodium phosphate as a buffer. Then the pH of the solution was adjusted by the addition of minute amounts of diluted phosphoric acid. The CD spectra immediately after sample preparation for the whole pH range examined (7.5–2.2) showed quite similar spectra with a large negative band around 198 nm, characteristic of a random coil conformation [21] (Figure 3A). After incubation at 37°C for 1 week, the CD spectra of samples above pH 5.0 remained unchanged (Figure 3B). On the other hand, at pH 4.5 and 4.1, the CD absorbance was reduced along the measured wavelength by the incubation, although random coil features in the CD spectrum were unchanged.

The decreases in the CD absorbance with incubation time can be considered to have arisen from the occurrence of large peptide aggregates which are undetectable by CD spectra. Since CD spectra could not determine the quantity of the aggregates, HPLC

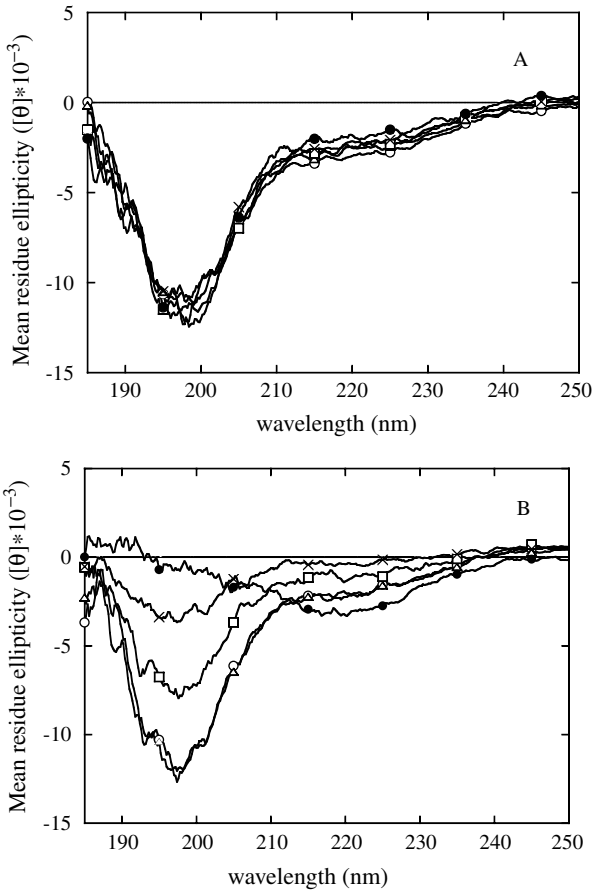


Figure 3 CD spectra of 1 mM NAC(1–13) with the pH adjusted from the neutral condition at 7.5. pH 7.5(○), 5.0(Δ), 4.5(□), 4.1(×) and 2.2(●). CD spectra of (A) were measured immediately after pH adjustment, and (B) were measured after 1 week of incubation at 37°C.

analyses were combined with CD measurements. The solute quantities were determined by HPLC peak area of filtrate samples through a 220 nm centrifugal filter. The CD intensity value at 198 nm ($\theta_{198}$) and the HPLC peak area of the filtrate sample at pH 7.5–4.1 were plotted against the incubation time in Figure 4A and B, respectively. The intensities immediately after the preparation at pH 7.5 were used as calibration values of 100%. The time dependence of $\theta_{198}$ was in good agreement with the solute quantity determined by HPLC (Figure 4A, B), indicating that over the pH range (7.5–4.1), the quantity of the random coil conformation correlates with the quantity of the soluble sample detected by HPLC. These results suggest that conformation of NAC(1–13) above pH 4.1 is only random coil, in spite of the aggregate occurrence.

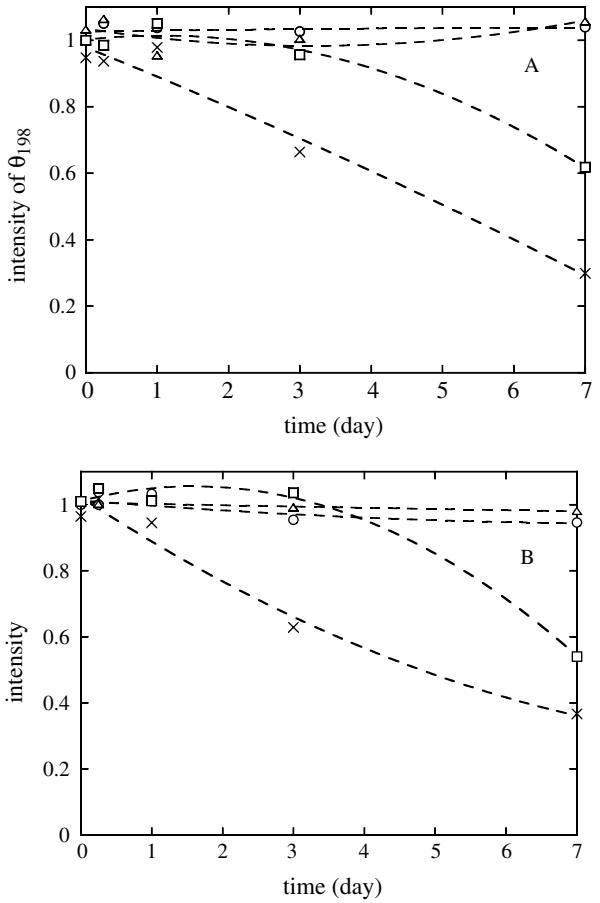


Figure 4 Comparison of CD intensity [$\theta_{198}$] and HPLC peak area of NAC(1–13). Each pH was adjusted from the neutral condition; pH 7.5(○), pH 5.0(Δ), pH 4.5(□) and pH 4.1(×). (A) $\theta_{198}$ intensity of the CD spectrum, and (B) solute quantity determined by HPLC are plotted against the incubation time of 0 h, 6 h, 1 day, 3 days and 7 days.

Unlike the samples above pH 4.1, some $\beta$-conformational features were observed in the CD spectrum for the sample at pH 2.2 during incubation (Figure 3B). This suggests that the secondary structure and aggregation process of NAC(1–13) are determined by the pH condition of the solution.

NAC(1–13) contains only three polar groups, the *N*-terminal amino group, the carboxyl group of E1 and the *C*-terminal carboxyl group of G13, whose polarity depend on the pH of the solution. To elucidate the cause of the pH-dependent aggregation of NAC(1–13), the three p$K_a$ values were determined by calculation of pH titration curves of $^1$H NMR chemical shifts (Figure 5). These p$K_a$s were determined to be $7.90 \pm 0.10$ for the *N*-terminal amino group, $4.10 \pm 0.03$ for the E1 carboxyl group and $3.62 \pm 0.03$ for the *C*-terminal carboxyl group.

Taking the CD and HPLC analyses into account, the conformation and aggregation process of NAC(1–13) according to the p$K_a$ value can be explained as follows: under the pH condition above the p$K_a$ of the E1 carboxylate group (>4.1), aggregation proceeds without obvious conformational conversion from the random coil in the sample solution. But under the pH condition with both carboxylate groups protonated at pH 2.2, $\beta$-conformational moiety slowly occurs in the sample during incubation (Figure 3A, B).

Under the neutral condition, NAC(1–13) did not aggregate despite incubation at 37 °C for 1 week, whereas NAC(1–18) in PBS solution formed fibrils and showed $\beta$-conformational CD spectra after a few days incubation at 37 °C [5]. Deletion of the hydrophobic *C*-terminal sequence VTAVA from NAC(1–18) may prevent NAC(1–13) from forming amyloid fibrils under the neutral condition.

## Aggregation Process of NAC(1–13) with the pH Adjusted from Acidic Condition

The CD spectra of NAC(1–13) directly set at acidic pH 2.2 showed a negative band near 218 nm and a positive band near 195 nm as evidence of $\beta$-conformation [21] (Figure 6), in contrast to the CD results with the pH adjusted from the neutral condition. On the other hand, the CD spectrum of the filtrate of a fresh solution at pH 2.2 through a 450 nm filter exhibited a random coil (Figure 6). The results revealed the co-existence of a random coil conformer and oligomerized $\beta$-conformational moiety in the 1 mM NAC(1–13) at pH 2.2.

Oligomerization of 1 mM NAC(1–13) at pH 2.2 was also verified by dynamic light scattering experiments. The mean diameter of the fresh solution of 1 mM NAC(1–13) at pH 2.2 was determined at 83.2 nm by volume-weighted gaussian analysis. The detailed data will be reported elsewhere.

The CD intensity at 218 nm ($\theta_{218}$), which is a good criterion for the peptide $\beta$-structure increased with incubation time (Figure 6). In contrast, $\theta_{198}$ and the HPLC peak area of filtrate of 1 mM NAC(1–13) at pH 2.2 decreased with the incubation time (data not shown). The results suggest that the increase of $\theta_{218}$ during the incubation results from the conversion of the random coil conformer to the $\beta$-conformation.

Temperature-melt CD spectra of freshly prepared 1 mM NAC(1–13) at pH 2.2 showed an isodichroic point at 203 nm, which provided evidence for a simple two-state $\beta$-sheet ⇔ random coil equilibrium (Figure 7).

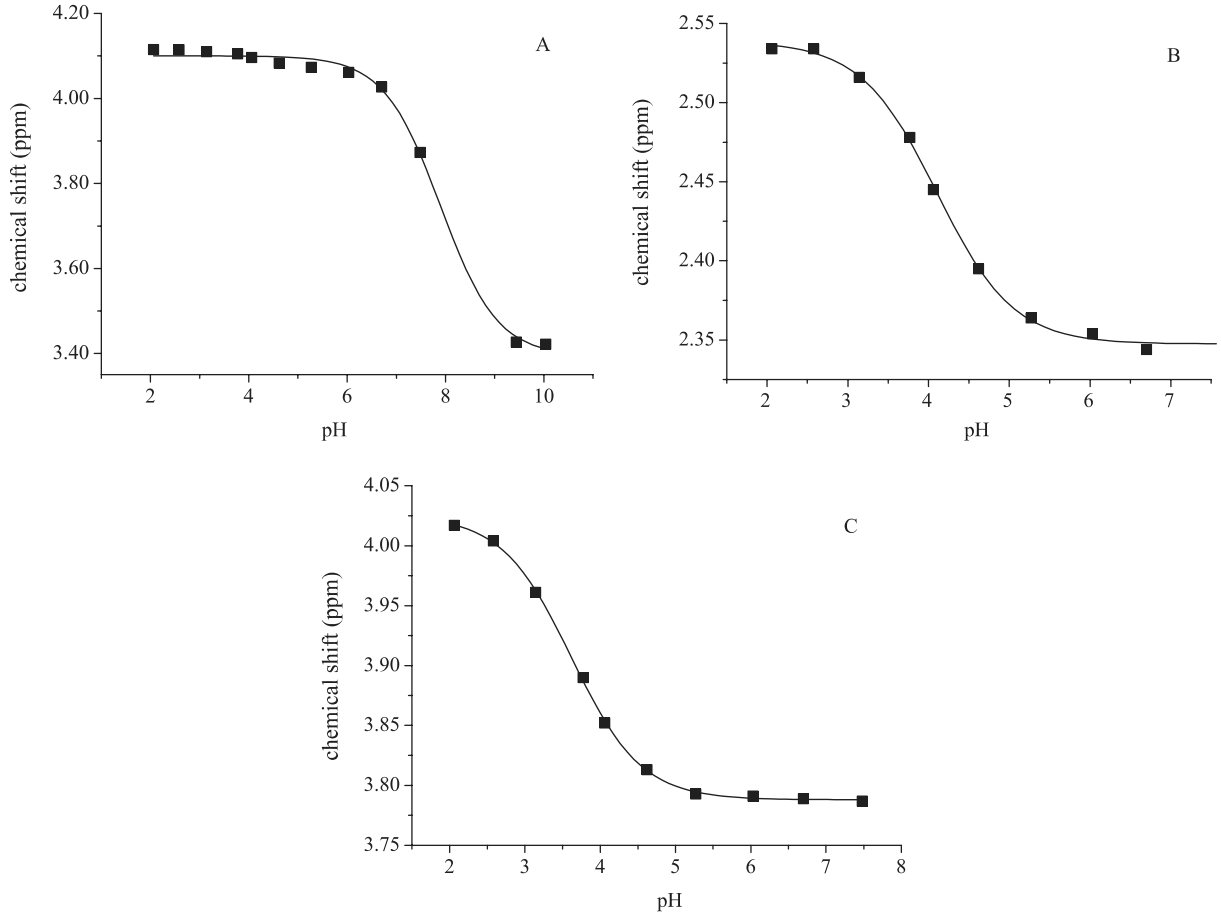


Figure 5 pH titration curves of (A) Glu1H$^{\alpha}$, (B) Glu1H$^{\gamma}$ and (C) Gly13H$^{\alpha}$ resonances. Chemical shifts extracted from 2D TOCSY experiments are plotted against the pH. The solid line was determined by nonlinear least-fitting of the experimental data to Eqn 1.

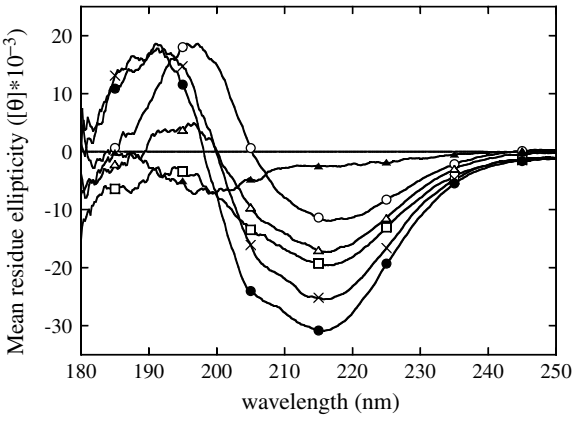


Figure 6 CD spectra of 1 mM NAC(1–13) with the pH immediately adjusted at 2.2, incubated at 37°C. Incubation time was (○) 0 h, (Δ) 6 h, (□) 1 day, (×) 3 days and (●) 7 days. CD spectrum of the filtrate immediately after preparation through 450 nm filter was shown (▲).

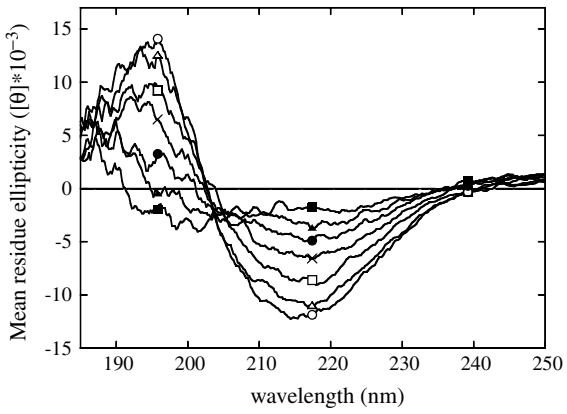


Figure 7 Temperature-melt CD spectra of 1 mM NAC(1–13) at pH 2.2 immediately after preparation between 25°C and 90°C. (○)25°C, (Δ)35°C, (□)45°C, (×)55°C, (●)65°C, (▲) 75°C and (■) 90°C.

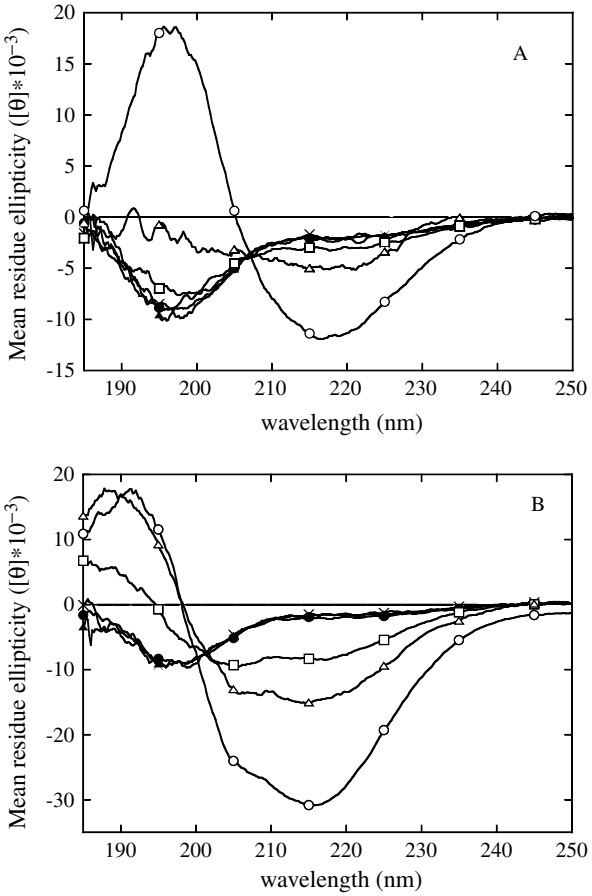


Figure 8 CD spectra of NAC(1–13) for the concentration range of 1000–31 μM at pH 2.2. (A) Immediately after sample preparation. (B) After incubation for 1 week at 37°C. (○) 1 mM, (Δ) 500 μM, (□) 250 μM, (×) 125 μM, (●) 63 μM and (▲) 31 μM.

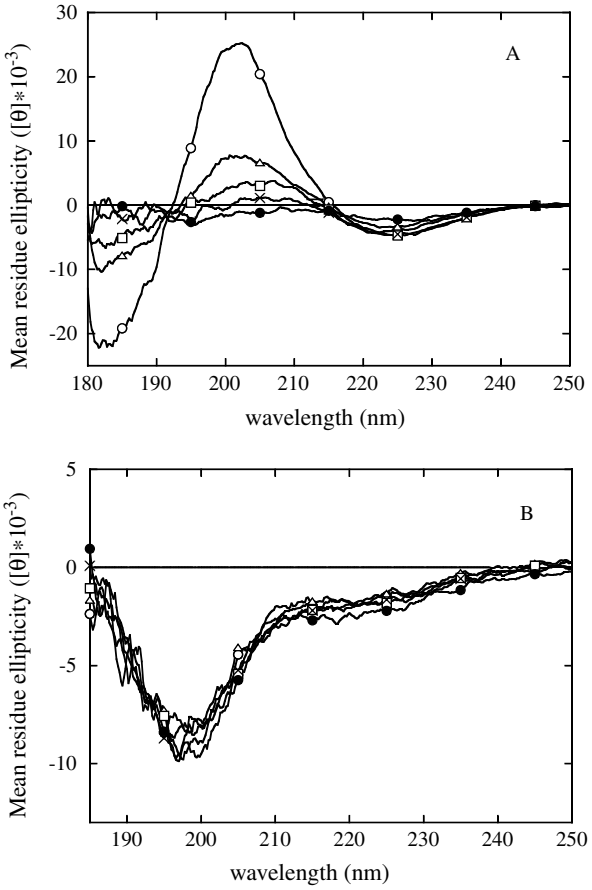


Figure 9 CD spectra of 1 mM NAC(1–13) with the pH adjusted from 2.2, incubated at 37°C. (A) pH 4.5. (B) pH 7.0. Incubation time was (○) 0 h, (Δ) 6 h, (□) 1 day, (×) 3 days and (●) 7 days.

Concentration-dependent CD spectra of NAC-(1–13) at acidic conditions at pH 2.2 immediately after preparation and incubated at 37°C for 1 week are shown in Figure 8A and B. The CD spectra immediately after preparation also showed an isodichroic point at 207 nm indicating a concentration-dependent $\beta$-sheet ⇔ random coil equilibrium (Figure 8A). Although CD spectra over the concentration of 31–125 μM remained unchanged despite 1 week of incubation at 37°C (Figure 8B), the CD spectrum of the 250 μM sample was distinctly converted from the random coil to $\beta$-conformation during incubation. At 500 μM, a considerable increase of $\theta_{218}$ was observed. The observed secondary structures are concentration-dependent, indicating that the oligomerization of the NAC(1–13) sample directly set to acidic pH 2.2 is responsible for the $\beta$-structure formation.

Unlike the sample at pH 4.5 adjusted from the neutral condition, the CD spectra of 1 mM NAC(1–13) at pH 4.5 adjusted from a more acidic condition pH 2.2 did not show the random coil feature (Figure 9A). The negative minimum near 225 nm and the positive maximum near 203 nm indicate the existence of $\beta$-conformation. The spectral intensity was distinctly reduced by incubation all along the observed wavelength probably due to the occurrence of the aggregation. The CD spectrum at pH 7.0 adjusted from pH 2.2 did not change after 1 week of incubation at 37°C (Figure 9B), similar to the samples above pH 5.0 with the pH adjusted from the neutral condition.

## pH-dependent Aggregation Mechanism of NAC(1–13)

The concentration dependent CD spectra showed that the $\beta$-conformational moiety is rapidly

 

generated under conditions of 1 mM at pH 2.2, and the $\beta$-conformational moiety is easily destabilized by dilution below 125 μM. These results indicate that oligomerization is necessary to stabilize the $\beta$-conformational moiety. In the studies of the molecular mechanism of the amyloid formation, it has been established that the polymerization process comprises two distinct processes that is, the nucleation and elongating growth of the fibrils [22,23]. Considering that the CD spectrum of NAC(1–13) at a concentration below 125 μM did not change despite 1 week of incubation at 37°C, it is suggested that the oligomerized $\beta$-conformational moiety functions as a nucleus for the fibril formation.

Since the aggregate forms are strongly influenced by the sample dissolution condition in spite of the same pH condition at 4.5, it is reasonable to consider that the $\beta$-conformational oligomers are responsible for fibril formation under the acidic condition. Under the solution condition of 1 mM NAC(1–13) directly set to pH 2.2, pre-existing $\beta$-conformational oligomer can play a role in the nucleus, and protofibrils grow by binding of random coil monomers to oligomer or protofibril ends. However, it is not clear at present whether the fibrils and ribbons are formed via the protofibril or not.

Recent studies on fibril-forming protein showed that the partially unfolded protein is ascribed to the nucleus of the amyloid formation [14,24,25]. In the study of A$\beta$ fibrillogenesis, the peptide micelle was proposed as another nucleus species due to its surfactant properties [13,26]. The micelle occurs when the peptide concentration is higher than the critical micelle concentration. Under this condition, a reversible equilibrium between monomers and micelles is rapidly established. When the peptide concentration is lower than the critical micelle concentration, no micelles are formed. Considering the property of fibril nucleus and sensitivity of the secondary structure to the sample concentration, the $\beta$-conformational oligomers of NAC(1–13) may be micelle-like as shown in the literature [13,26,27].

Unlike the samples prepared from a more acidic condition, the sample solutions of NAC(1–13) at pH 4.5 and 4.1 prepared from the neutral condition formed aggregates without fibril formation and without distinct conformational conversion from the random coil. Taking the EM results into account, it can be concluded that the aggregates of NAC(1–13) formed in the sample with the pH adjusted from the neutral condition to 4.1 and 4.5 are unable to function as a nucleus of the fibril formation. Since the p$K_a$ of the carboxyl group of E1 is 4.1, the occurrences of the aggregate at pH 4.5 and 4.1 are attributed to protonation of the carboxyl group of E1. Thus, it is reasonable to consider that the E1 protonated NAC(1–13) (the *N*-terminal amide and *C*-terminal carboxylate group are charged) can play a role as the nucleus in the amorphous aggregate formation, but can not do so in the fibril formation.

In this study of NAC(1–13), it has been shown that the aggregate morphology of NAC(1–13) strongly depended on the pH condition immediately after sample dissolution. A similar difference of aggregate morphology depending on the solution pH was also reported for an other fibril-forming peptide. Wood *et al.* showed that the aggregate of A$\beta$ at pH 5.8 was incapable of seeding for fibril growth at pH 7.4 [16]. From the viewpoint of physiology, it is important to consider the influence of pH on fibrillogenesis because there is a subtle difference of pH in each organelle.

For the sample of 1 mM NAC(1–13) at pH 2.2, the CD data indicated the existence of $\beta$-conformational oligomers immediately after preparation, and EM and Congo red birefringence experiments revealed the amyloid fibril after 1 week of incubation. On the studies of fibril-forming protein, partially unfolded protein is ascribed to the nucleus of the amyloid formation [14,24,25]. Unlike protein, peptide is unfolded by nature. Thus, it can be suggested that the formation of $\beta$-conformational oligomer is an essential process for the fibril formation of a peptide such as NAC(1–13).

## Acknowledgement

The authors would like to thank Mr Y. Satoh and T. Suzuki of Jeol Ltd for their help with EM observations.

## REFERENCES

1. Kelly JW, Colon W, Lai Z, Lashuel HA, Mcculloch J, Mccutchen SL, Miroy GJ, Peterson SA. Transthyretin quaternary and tertiary structural changes facilitate misassembly into amyloid. *Adv. Protein Chem.* 1997; **50**: 161–181.
2. Carrell RW, Gooptu B. Conformational changes and disease — serpins, prions and Alzheimer's. *Curr. Opin. Struct. Biol.* 1998; **8**: 799–809.

 

3. Iwai A, Yoshimoto M, Masliah E, Saitoh T. Non-A$\beta$ component of Alzheimer's disease amyloid (NAC) is amyloidogenic. *Biochemistry* 1995; **34**: 10139–10145.
4. El-Agnaf OMA, Jakes R, Curran MD, Middleton D, Ingenito R, Bianchi E, Pessi A, Neill D, Wallace A. Aggregates from mutant and wild-type $\alpha$-synuclein proteins and NAC peptide induce apoptotic cell death in human neuroblastoma cells by formation of $\beta$-sheet and amyloid-like filaments. *FEBS Lett.* 1998; **440**: 71–75.
5. El-Agnaf OMA, Bodles AM, Guthrie DJS, Harriott P, Irvine GB. The *N*-terminal region of non-A$\beta$ component of Alzheimer's disease amyloid is responsible for its tendency to assume $\beta$-sheet and aggregate to form fibrils. *Eur. J. Biochem.* 1998; **258**: 157–163.
6. Bodles AM, Guthrie DJS, Harriott P, Campbell P, Irvine GB. Toxicity of non-A$\beta$ component of Alzheimer's disease amyloid, and *N*-terminal fragments thereof, correlates to formation of $\beta$-sheet structure and fibrils. *Eur. J. Biochem.* 2000; **267**: 2186–2194.
7. Ueda K, Fukushima H, Masliah E, Xia Y, Iwai A, Yoshimoto M, Otero DAC, Kondo J, Ihara Y, Saitoh T. Molecular cloning of cDNA encoding an unrecognized component of amyloid in Alzheimer disease. *Proc. Natl Acad. Sci. USA* 1993; **90**: 11282–11286.
8. Han H, Weinreb PH, Lansbury PT Jr. The core Alzheimer's peptide NAC forms amyloid fibrils which seed and are seeded by $\beta$-amyloid: is NAC a common trigger or target in neurodegenerative disease? *Chem. Biol.* 1995; **2**: 163–169.
9. Ueda K, Saitoh T, Mori H. Tissue-dependent alternative splicing of mRNA for NACP, the precursor of non-A$\beta$ component of Alzheimer's disease amyloid. *Biochem. Biophys. Res. Commun.* 1994; **205**: 1366–1372.
10. Spillantini MG, Schmidt ML, Lee VM, Trojanowski JQ, Jakes R, Goedert M. $\alpha$-synuclein in Lewy bodies. *Nature* 1997; **388**: 839–840.
11. Polymeropoulos MH, Lavedan C, Leroy E, Ide SE, Dehejia A, Dutra A, Pike B, Root H, Rubenstein J, Boyer R, Stenroos ES, Chandrasekharappa S, Athanassiadou A, Papapetropoulos T, Johnson WG, Lazzarini AM, Duvoisin RC, Di Iorio G, Golbe LI, Nussbaum RL. Mutation in the $\alpha$-synuclein gene identified in families with Parkinson's disease. *Science* 1997; **276**: 2045–2047.
12. Kruger R, Kuhn W, Muller T, Woitalla D, Graeber M, Kosel S, Przuntek H, Epplen JT, Schols L, Riess O. Ala30Pro mutation in the gene encoding $\alpha$-synuclein in Parkinson's disease. *Nat Genet.* 1998; **2**: 106–108.
13. Lomakin A, Chung DS, Benedek GB, Kirschner DA, Teplow DB. On the nucleation and growth of amyloid $\beta$-protein fibrils: Detection of nuclei and quantitation of rate constants. *Proc. Natl Acad. Sci. USA* 1996; **93**: 1125–1129.
14. McParlard VJ, Kad NM, Kalverda AP, Brown A, Kirwin-Jones P, Hunter MG, Sunde M, Radford SE. Partially unfolded states of $\beta_2$-microglobulin and amyloid formation *in vitro*. *Biochemistry* 2000; **39**: 8735–8746.
15. Guijarro JI, Sunde M, Jones JA, Campbell ID, Dobson CM. Amyloid fibril formation by an SH3 domain. *Proc. Natl Acad. Sci. USA* 1998; **95**: 4224–4228.
16. Wood SJ, Maleeff B, Hart T, Wetzel R. Physical, morphological and functional differences between pH 5.8 and 7.4 aggregates of the Alzheimer's amyloid peptide A$\beta$. *J. Mol. Biol.* 1996; **256**: 870–877.
17. Fraser PE, Nguyen JT, Surewicz WK, Kirschner DA. pH-dependent structural transitions of Alzheimer amyloid peptides. *Biophys. J.* 1991; **60**: 1190–1201.
18. Lashuel HA, LaBrenz SR, Woo L, Serpell LC, Kelly JW. Protofilaments, filaments, ribbons, and fibrils from peptidomimetic self-assembly: Implications for amyloid fibril formation and materials science. *J. Am. Chem. Soc.* 2000; **122**: 5262–5277.
19. Wüthrich K. *NMR of Proteins and Nucleic Acids*. Wiley: New York, 1986.
20. Forman-Kay JD, Clore GM, Gronenborn AM. Relationship between electrostatics and redox function in human thioredoxin: Characterization of pH titration shifts using two-dimensional homo- and heteronuclear NMR. *Biochemistry* 1992; **31**: 3442–3452.
21. Fasman GD (ed.). *Circular Dichroism and the Conformational Analysis of Biomolecules*. Plenum Press: New York, 1996.
22. Jarrett JT, Lansbury PT Jr. Seeding 'one-dimensional crystallization' of amyloid: A pathogenic mechanism in Alzheimer's disease and scrapie? *Cell* 1993; **73**: 1055–1058.
23. Harper JD, Lansbury PT Jr. Models of amyloid seeding in Alzheimer's disease and scrapie: Mechanistic truths and physiological consequences of the time-dependent solubility of amyloid proteins. *Annu. Rev. Biochem.* 1997; **66**: 385–407.
24. Booth DR, Sunde M, Bellotti V, Robinson CV, Hutchinson WL, Fraser PE, Hawkins PN, Dobson CM, Radford SE, Blake CCF, Pepys MB. Instability, unfolding and aggregation of human lysozyme variants underlying amyloid fibrillogenesis. *Nature* 1997; **385**: 787–793.
25. Baskakov IV, Legname G, Prusiner SB, Cohen FE. Folding of prion protein to its native $\alpha$-helical conformation is under kinetic control. *J. Biol. Chem.* 2001; **276**: 19687–19690.
26. Lomakin A, Teplow DB, Kirschner DA, Benedek GB. Kinetic theory of fibrillogenesis of amyloid $\beta$-protein. *Proc. Natl Acad. Sci. USA* 1997; **94**: 7942–7947.
27. Serio TR, Cashikar AG, Kowal AS, Sawicki GJ, Moslehi JJ, Serpell L, Arnsdorf MF, Lindquist SL. Nucleated conformational conversion and the replication of conformational information by a prion determinant. *Science* 2000; **289**: 1317–1321.

 